A Multi-Beam Circularly Polarized Fabry-Perot Resonator Antenna Array Using SIW for X-Band Applications

Reza Khajeh Mohammad Lou[1&2], Tohid Aribi[1&2*] Tohid Sedghi[3&4] and Bal S. Virdee[5]

[1] Department of Electrical Engineering, Miandoab Branch, Islamic Azad University, Miandoab, Iran
[2]Artificial Intelligence and Big data Automation Research Center, Urmia Branch, Islamic Azad University, Urmia, Iran
[3] Department of Electrical Engineering, Urmia Branch, Islamic Azad University, Urmia, Iran
[4] Microwave and Antenna Research Center, Urmia Branch, Islamic Azad University, Urmia, Iran
[5] Center for Communications Technology London, Metropolitan University, London, U.K.

corresponding author: tohidaribi@gmail.com

Abstract

This paper presents a novel multi-layer beamforming antenna array based on Fabry-Perot resonator that is excited by a high-performance compact 4×4 Butler matrix using substrate integrated waveguide (SIW) technology for X-band application. The adapted ring patch antenna is fed through the aperture on a rectangular SIW cavity and forms the radiating element in the antenna array. Enhanced characteristics of the antenna array are realized by inserting an electromagnetic bandgap (EBG) structure between the radiating elements and a superstrate constituted from two complementary frequency selective surfaces (FSS) that forms a Fabry-Perot resonator (FPR). Circular polarization in the proposed FPR SIW antenna array (FPRSAA) is achieved by using a combination of sequential phase rotation and orthogonal feeding techniques. Measured results of antenna array (Ant. II) show $|S_{11}| \leq -10$ dB between 8-12.0 GHz, a circular polarization (CP) gain variation between 15.64-18.54 dBic, 3 dB axial-ratio between 8.5-11 GHz, and scanning angle covering -47 to 47 degrees.

1. Introduction

Terrestrial and spaceborne tracking systems require a wide beamwidth and capability to manage high data rates [1-3]. However, wide beamwidth antennas have a low gain. This means that high data rate communications link between fast-moving objects like an aircraft and a satellite cannot be maintained reliably [4,5]. It is highly challenging to realize antennas that possess concurrent characteristics of wide beamwidth and high gain using standard antenna techniques. It is proposed here that the above characteristics can be achieved with antennas that possess beam steering capability such as phase array or switched multibeam antennas. Switched multibeam antennas are more popular than phased array antennas due to their cost-effective implementation that do not require electronic phase shifters [6-8].

Various beam forming networks (BFNs), such as Butler, Blass, and Nolen Matrix, can be used to achieve the functionality of switched beamforming in antenna arrays [9-11]. Among the BFNs, the Butler Matrix is popular due to its moderate complexity and good performance. It consists of N×N input/output ports producing N beams in different directions. Nevertheless, the conventional Butler Matrix with microstrip technology has some drawbacks, such as low isolation between adjacent ports, large size, narrow bandwidth, and the inherent limitation of microstrip technology at upper microwave frequencies for high-power applications. In addition, microstrip structures are limited by frequency dependence and substrate parameters such as relative electrical permittivity and loss tangent [12,13]. However, substrate integrated waveguide (SIW) technology can be used to overcome these disadvantages, which combines the advantages of low manufacturing cost in

the printed circuit board (PCB) technology and low loss of waveguide structures. Unlike traditional waveguides, a SIW is composed of a thin dielectric substrate covered on both faces by a metallic layer and studded at the periphery with metallic via holes rather than the solid walls [14-16].

Various methods have been used to increase the gain of antenna arrays, including electromagnetic bandgap (EBG) structures [17,18]. The EBG have been used successfully to suppress the propagation of surface waves between radiating elements in array antennas. Partially reflective surfaces (PRS) of EBG can be used to create a superstrate that can concentrate radiation energy in a specific direction. These antennas are commonly referred to as Fabry-Perot resonator (FPR) antennas [19,20].

Signals propagating in free-space experience multipath fading and polarization mismatch between wireless transceivers, which can significantly impact their performance. To mitigate the effects of polarization distortion the antenna must be able to circularly polarize transmissions. Various methods have been proposed in the literature to obtain circular polarization that include sequential phase rotation technique, circularly polarized FPR, and orthogonal feeding techniques [21,22].

This paper describes a SIW Butler Matrix with improved characteristics to feed radiating elements in antenna arrays. Three different configurations of the proposed antenna array are presented here to show the improvement of the antenna's performance. The prototype of the antenna array was fabricated to verify its performance. The results show that the antenna array has an impedance bandwidth for $|S_{11}|$<-10 dB of 4 GHz between 8-12 GHz, a 3 dB CP gain bandwidth of 2.5 GHz between 8.5-11 GHz with a maximum value of 18.2 dBic, and a 3 dB axial-ratio (AR) bandwidth of 3.4 GHz between 8.1-11.5 GHz. Also, the proposed antenna has a suitable scanning angle range from -47 to 47 degrees. These characteristics make the antenna suitable for application at X-band satellite and radar systems.

2. Beamforming Network Configuration

The proposed multi-layer 2×2 low-cost switched-beam antenna array fed by a 4×4 SIW Butler Matrix is shown in Fig.1. The configuration of the 4×4 Butler matrix has been selected as the beamforming network for the switched-beam antenna array. The BFN is implemented such that, in addition to eliminating crossovers in conventional Butler Matrix configuration, it improves the circular polarization behavior of the antenna array by applying sequential rotating feeding technique and a quadrature phase shift between the output ports. The proposed BFN consists of four SIW cross couplers that form a 4×4 network. The phase difference is obtained using unequal length phase shifters in the Butler Matrix. The proposed antenna array comprises:

I) Butler Matrix feeding network on the first layer. The BFN uses SIW cross couplers.
II) SIW interface between the BFNs and the 2×2 radiation elements implemented on the second layer (Ant. 0).
III) Embedded on the third layer are the 2×2 radiation elements consisting of modified ring patch antennas (MRPA) which are fed through the aperture constructed on the second layer. The array of EBG unit cells is used to reduce the mutual coupling between adjacent antennas (Ant. I).
IV) Finally, the proposed Fabry-Perot resonator antenna array (Ant. II) is constituted from a superstrate consisting of hexagonal patches and a hexagonal aperture located on top of the radiating elements.

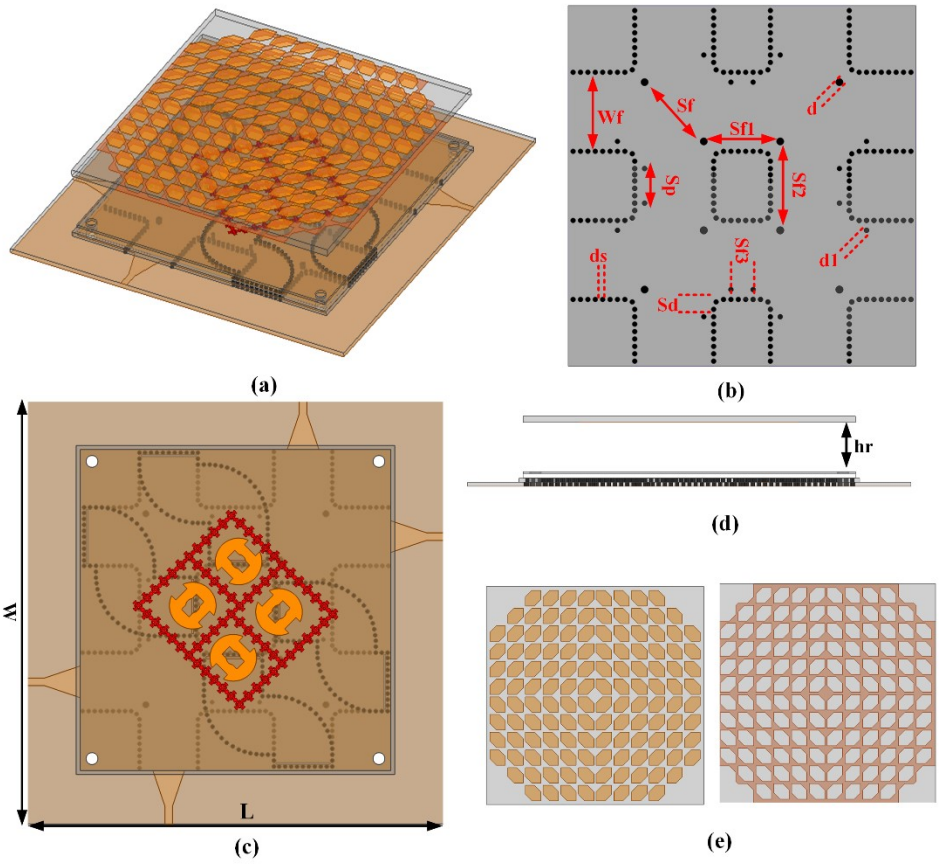

Fig. 1 Geometry of proposed antenna array, (a) 3D view of final configuration, (b) Feeding network, (c) Top view without PRS, (d) Side view with PRS, and (e) PRS configuration.

The number of PRS unit cells (n) was calculated by dividing the effective radiating aperture of the antenna (A) with the area of each unit cell (A_{UC}), i.e., $n = A/A_{UC}$. Aperture area was calculated by first determining the directivity of PRS superstrate (D_{PRS}) using [23,24]

$$D_{PRS} = 10Log\frac{1+\Gamma}{1-\Gamma} \qquad (1)$$

Where Γ is the reflection coefficient of the unit cell. Then the directivity of the proposed Fabry-Perot resonator antenna (D_{FPRA}) was determined by summing D_{PRS} and the directivity of antenna without superstrate (D_{REF}) expressed as $D_{FRPA} = D_{PRS} + D_{ref}$. The aperture size of the antenna was then calculated using [23,24]

$$A = \frac{10^{\frac{D_{FPRA}}{10}}\lambda^2}{\pi^2} \qquad (2)$$

where λ is the operating wavelength.

Fig.2 shows the simulated S-parameters and the phase difference response between the output ports of the SIW cross coupler. The SIW cross coupler exhibits transmission between the ports #1

& #2 and ports #1 & #3 with a phase difference of 90 degrees between 8-11.4 GHz. The input power is approximately equally divided between ports #2 & #3. The return-loss at port 1 is better than -10 dB. The signal between ports #1 & #4 is attenuated more than 10 dB and the attenuation is maximum of 45 dB at 10.3 GHz.

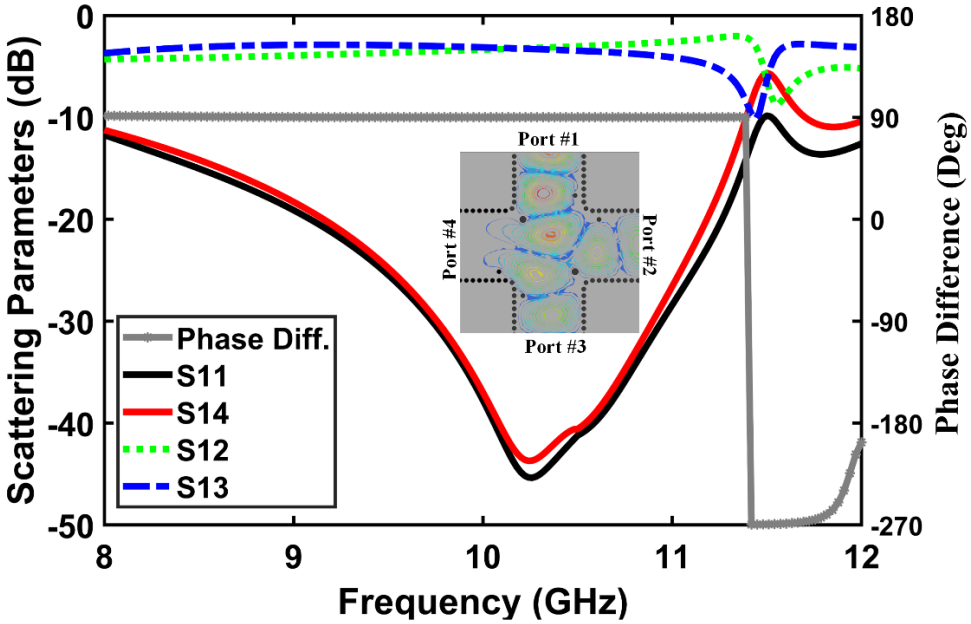

Fig. 2 Scattering parameters and phase difference response of the SIW cross coupler.

Simulated scattering parameters of the BFN, i.e., the return-loss, the insertion-loss, and phase are shown in Figs. 3 and 4, when ports #1 & #2 are excited. Fig. 3 shows the impedance bandwidth for $|S_{11}|$ & $|S_{22}| \leq$ -10 dB is 3.4 GHz from 8-11.4 GHz, which covers 85% of the X-band. Total coverage over the X-band is achieved for $|S_{11}|$ & $|S_{22}| \leq$ -7 dB. The simulated phase responses at the output ports relative to the two input ports #1 & #2 (P1 & P2) are shown in are shown in Fig. 4. The phase angle varies between ±174°. At 10 GHz, relative to port #1 the phase at port #5 is 0 °, port #6 is -91°, port #7 is 50°, and port #8 is -30°. Similarly, at 10 GHz, relative to port #2 the phase at port #5 is 83°, port #6 the phase varies between ±174°, port #7 is 130°, and port #8 is 34°.

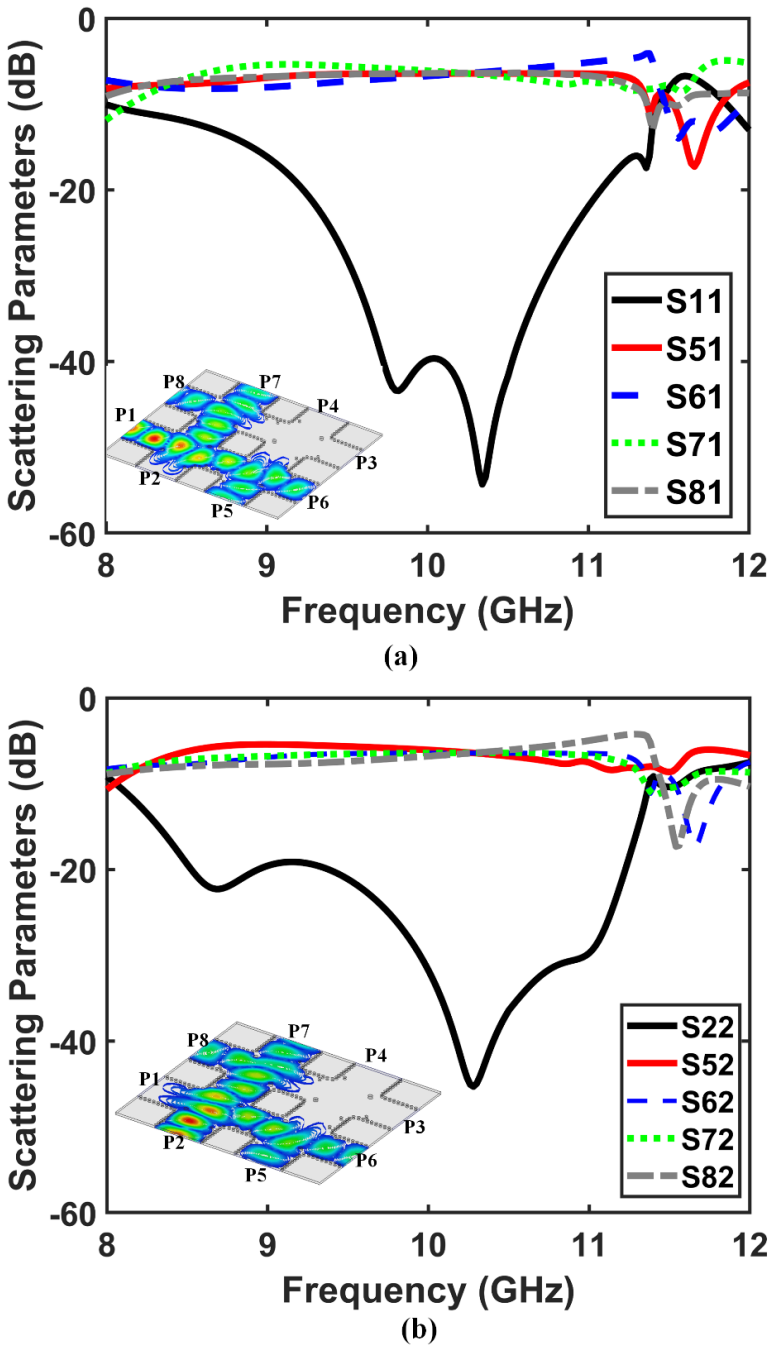

Fig. 3 Simulated results of SIW BFN, (a) insertion loss and return loss at port #1, and (b) insertion loss and return loss at port #2.

The 4×4 SIW Butler Matrix was fabricated on a commercially available substrate (RO4003C) with a relative permittivity of 3.55 and dimensions of 78×81×1 mm^3. The optimized SIW BFN dimensions are as follows (units: mm): $W_f = 15$, $S_f = 16$, $S_{f1} = 15$, $S_{f2} = 18$, $S_{f3} = 4.5$, $d = 1.5$, $d_1 = 1$, $d_s = 1$, $S_p = 7$, and $S_d = 3.5$. These parameters are annotated in Fig.1(b).

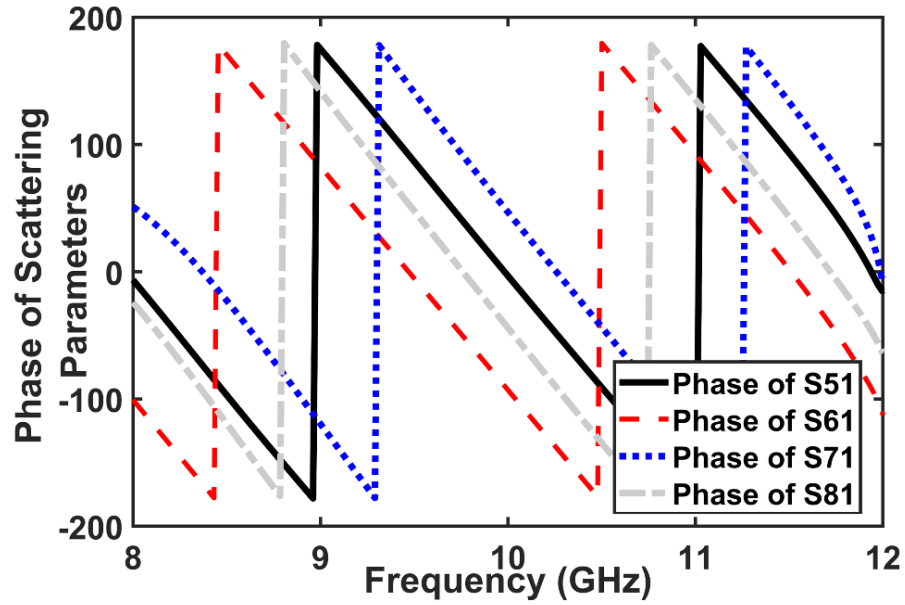

(a)

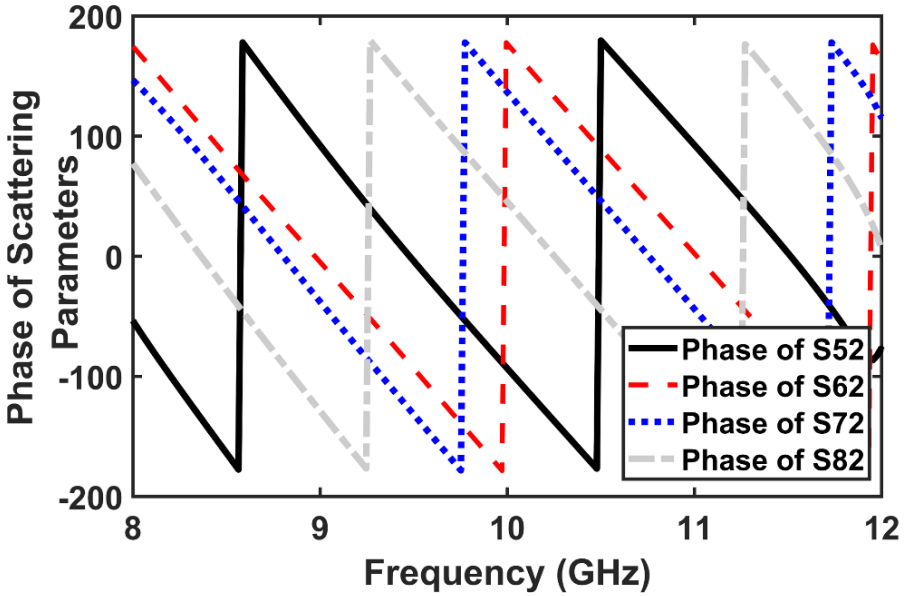

(b)

Fig. 4 Simulated phase progression of SIW BFN at output ports, (a) port #1 (P1), and (b) port #2 (P2).

3. Antenna Array Design

3.1. Radiating Element Configuration

Choosing a radiation element for an array antenna is important as it determines the performance of an antenna array. Moreover, the loss of the antenna's feed network should be minimal. The radiation element's performance is determined by various factors including its impedance bandwidth, antenna gain, and axial ratio. These characterizing parameters define the characteristics of beamforming antenna arrays.

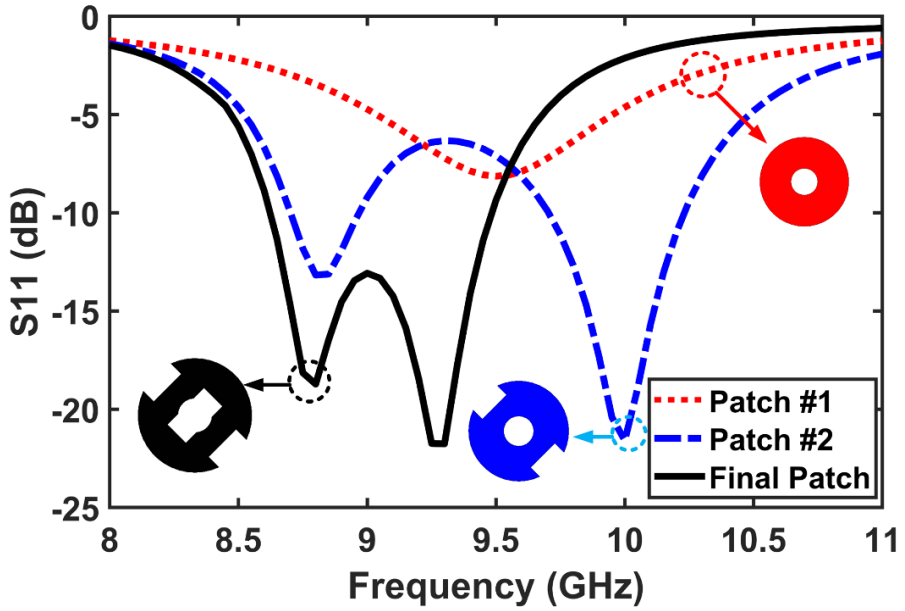

Fig. 5 Return loss responses of various modified ring patch antennas (MRPA).

The geometry of the proposed antenna was obtained through a step-by-step process as follows:

1. Design and construction of a circular ring with a certain inner and outer radius for operation at a specified frequency, in this case 9 GHz.
2. Modification of the circular ring by cutting out rectangular slots at the outer peripherals of the ring to excite two resonance modes, in this case at 8.7 & 10 GHz, as inset in Fig.5.
3. A rectangular slot is cutout in the center of the circular ring, as inset in Fig.5. The width of the rectangular cutout is smaller than the diameter of the inner ring for the structure to exhibit improved impedance bandwidth and promote circular polarization.

In this work, the modified ring patch antenna (MRPA) shown in Fig.5 was used as a radiating element. For experimental purpose MRPA was constructed on top of a rectangular SIW cavity with a rectangular aperture to excite the antenna. The SIW structure was implemented using Rogers RT/ Duroid 4003 substrate with $\varepsilon_r = 3.55$ and $\tan\delta = 0.0027$. The top and bottom layers had a thickness of 1 mm and 0.5 mm, respectively. The air gap between the two layers of 1 mm, which was chosen to provide a wide impedance bandwidth.

The MRPA configuration dimensions are as follows (Units: mm): $W_{sub} = 20$, $L_{sub} = 35$, $R_s = 6$, $L_s = 4.1$, $L_r = 2.75$, $W_s = 15$, and $\Theta = 45^o$. The proposed MRPA antenna geometry was optimized by a parametric study using CST Microwave Studio ver. 2018. The surface current distribution arrows on the proposed antenna rotate as a function of time, as shown in Fig.6, which is characteristic of circular polarization.

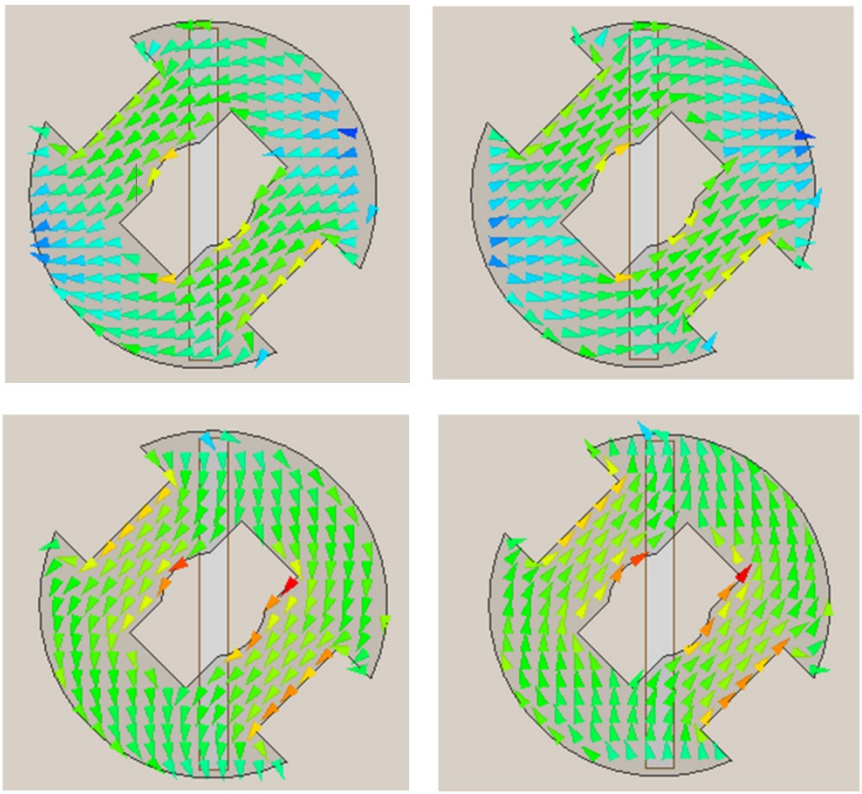

Fig. 6 Surface current rotation as a function of time over the proposed radiating element at 9 GHz.

Fig.5 shows how the return loss of the ring resonator patch varied as it was modified. The final patch had an impedance bandwidth of 0.85 GHz between 8.65 GHz to 9.5 GHz for $|S_{11}| \leq -10$ dB. Figs.7 to 8 show the simulated return-loss ($|S_{11}|$), antenna gain, axial-ratio, and radiation pattern of the antenna. The antenna gain in Fig.7 is almost flat from 8.5 GHz to 9.5 GHz with a peak value of 8.2 dB across 8.8 GHz and 9.25 GHz. The axial ratio the antenna varies between 1.1 dB and 5 dB and it has a 3 dB bandwidth of 800 MHz. The antenna's radiation pattern at 8.8 GHz and 9.25 GHz are shown in Fig.8 for phi equal to 0^{o} (E-plane) and 90^{o} (H-plane). The radiation patterns are nearly semi-directional in the E-plane and H-plane.

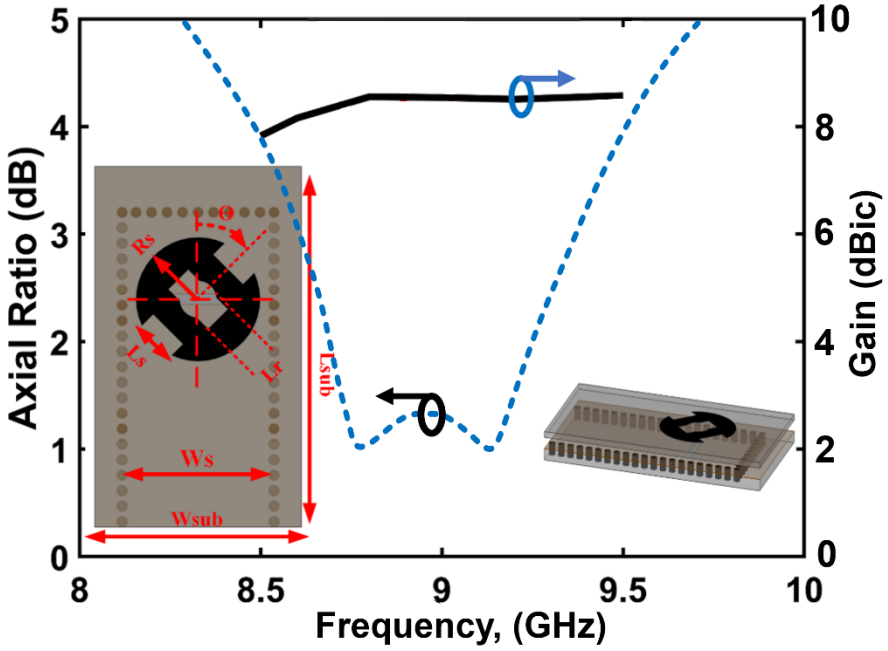

Fig. 7 Geometry of MRPA and the antenna gain and axial ratio as a function of frequency.

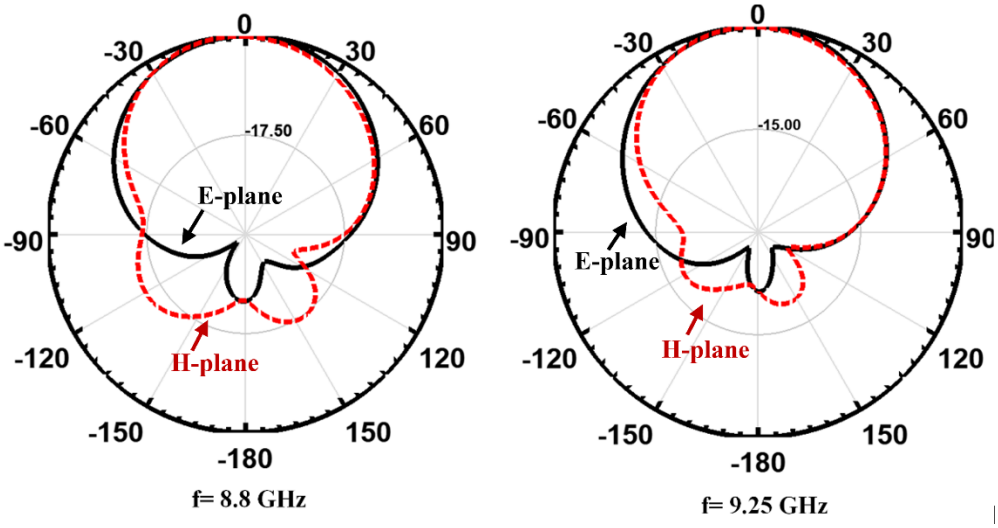

Fig. 8 Radiation pattern of MRPA for phi = 0° and phi = 90° at f = 8.8 GHz and 9.25 GHz.

3.2. Electromagnetic Bandgap Structure

One of the issues encountered with antenna arrays is adverse effects of surface waves resulting from near field mutual coupling between adjacent antennas, which can dramatically compromise the performance of the array. Various methods have been proposed to solve this issue. One of the most common methods is the use of electromagnetic bandgap structures (EBG) placed between radiating elements of the antenna array. In recent years, much research has been done on EBG structures, and various EBG configurations have been considered. Among them includes the

uniplanar electromagnetic bandgap (UC-EBG) structure, which has received great attention due to its simplicity and integration with microwave circuits [25-27].

In this paper, a new UC-EBG structure is introduced for application at X-band, which is shown in Fig.9. The proposed UC-EBG is a cross shaped structure with T-shaped arms and curved stubs. The curved stubs resemble a broken circle on which the cross is placed. The unique structure provides a low impedance path to ground for surface waves, and thereby preventing interaction between two neighboring ports over a wideband. Moreover, this is achieved with just a few UC-EBGs. The UC-EBG was constructed on Rogers RT/ Duroid 4003 substrate with permittivity of 3.55 and thickness is 0.5 mm. The optimized dimensions of the UC-EBG are (units: mm): W_E = 2.97, R_E = 0.95, W_{E1} = 0.33 and L_E = 1.0.

To investigate the characteristics of the proposed UC-EBG, a 1×4 array of this structure was located between two 50 Ω open-ended microstrip-lines, as shown in Fig.8(a). One of the microstrip-lines was used to excite surface waves and the other was used to measure the amount of coupled electromagnetic field. The current density distribution over the UC-EBG structure at 10 GHz is shown in Fig.9(a) where the red shaded regions represent high current density and the regions of green/blue indicate where the current density is low. Fig.9(b) shows the E-field between ports #1 & #2. Fig.9(c) shows the isolation between ports #1 and #2 to be greater than 40 dB. The isolation id greatest at 9.7 GHz. This demonstrates the effectiveness of the UG-EBG at blocking the transmission between ports #1 & #2 over a frequency range of 8-12 GHz.

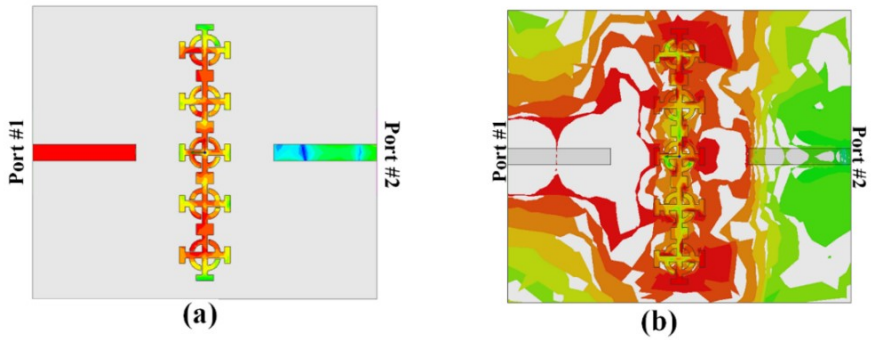

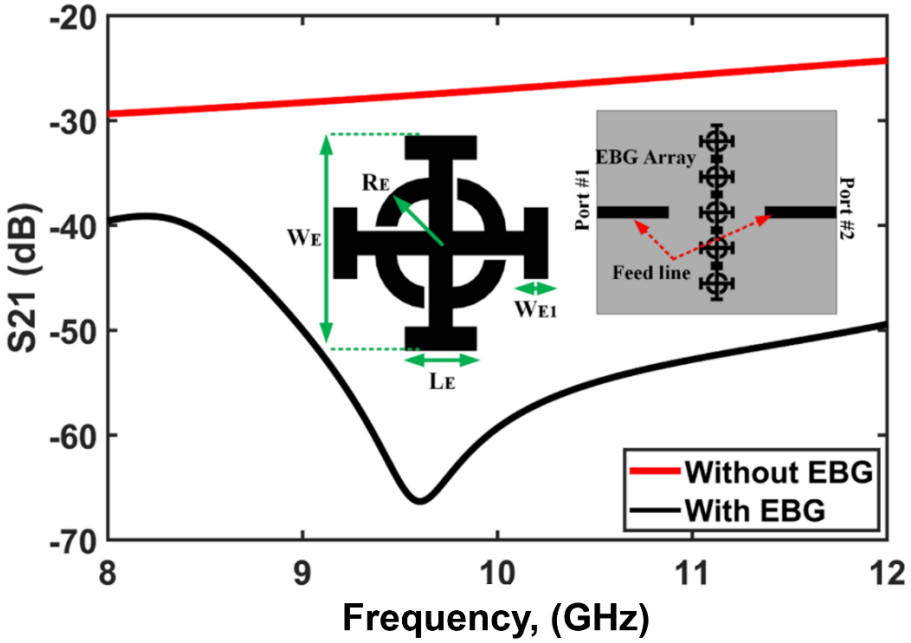

(c)

Fig. 9 UC-EBG, (a) Electrical field distribution, (b) current density distribution, and (c) geometry and simulated insertion-loss.

3.3. Partially Reflective Surface (PRS)

As mentioned earlier, one way to achieve high gain antennas is to use Fabry-Perot resonator (FPR) configuration. A conventional FPR is a superstrate made of a partially reflective surface located above the antenna ground. By increasing the reflection of PRS, a high gain antenna is obtained however at the cost of bandwidth reduction. It has been shown that a high gain and broadband performance can be achieved by using PRS with a positive phase gradient over the frequency range of interest [28,29]. Here we have used this technique to realize a wideband FPR antenna.

Fig.10 shows a hexagonal patch that is excited through a hexagonal aperture [30]. This structure was used as a unit cell of the PRS. The optimized dimensions of the PRS unit cell are (units: mm): t = 1.57, W_{f1} = 5.29, W_{f2} = 3.1, and W_{fa} = 6.0. CST Microwave Studio a 3D full-wave EM tool was used to analyze and optimize the PRS unit cell. Fig.11 shows the insertion-loss and the phase response of the PRS unit cell. The PRS exhibits a 180-degree reflective phase in the X-band.

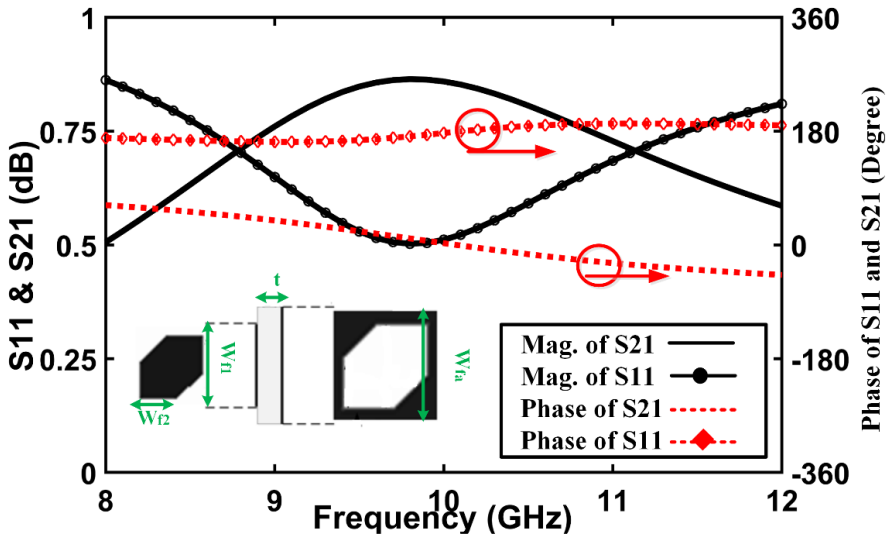

Fig. 10 Configuration of the PRF and its insertion loss and phase response.

4. Experimental Results:

To better understand the effect of UC-EBG and PRS separately, the array's performance was investigated by simulation and verified experimentally. Ant. 0 is the antenna array without UC-EBG and PRS, and Ant. I is an array with just the UC-EBG. Antenna array Ant. II has both UC-EBG and FPR, as shown in Fig.1. Multiple ripples are observed in the return loss response of Ant. 0 and Ant. I in Fig.11. These ripples result from wave reflections due to impedance mismatch at the antenna ports. However, as long as the return loss ripples are less than -10 dB over the bandwidth of the antenna the impedance matching is considered to be good and acceptable for practical applications. From Fig.11 the simulated impedance bandwidth of antenna array Ant. 0 for $|S_{11}| \leq$ -10dB when port #1 is excited is 3.4 GHz from 8.26 GHz to 11.66 GHz, which corresponds to a fractional bandwidth of 34%. In the case of Ant. I the impedance bandwidth is 3.66 from 8.12 GHz to 11.78 GHz, which corresponds to a fractional bandwidth of ~37%. When port #2 is excited, the impedance bandwidth for Ant. 0 and Ant. I are 2.3 GHz and 3.81 GHz, respectively, and the corresponds to a fractional bandwidths are 25% and 38%, respectively. These results show that by embedding UC-EBG between radiating elements, the resonance becomes stronger and impedance matching is improved. The antenna gains and axial ratio of Ant. 0 and Ant. I are shown in Fig.12 when port #1 is excited. The peak gain is 12.5 dBic for Ant. 0 and 14.43 dBic for Ant. I. The 3 dB axial ratio bandwidth of the Ant. 0 is ~1.9 GHz, and 2.1 GHz for Ant. II. Note that the circular polarization for Ant. 0 is ~47% and 52% for Ant. I. This shows that the UC-EBG structure applied to Ant. I has the benefit of increasing the antenna gain as well as improve CP bandwidth.

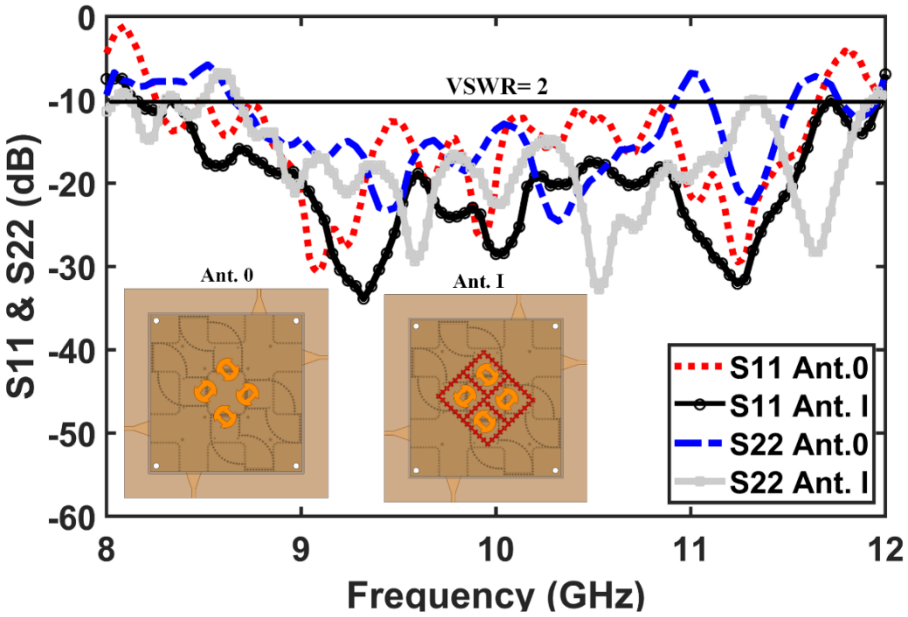

Fig. 6 Simulated return-loss of Ant.0 and Ant. I when ports #1 and #2 are excited.

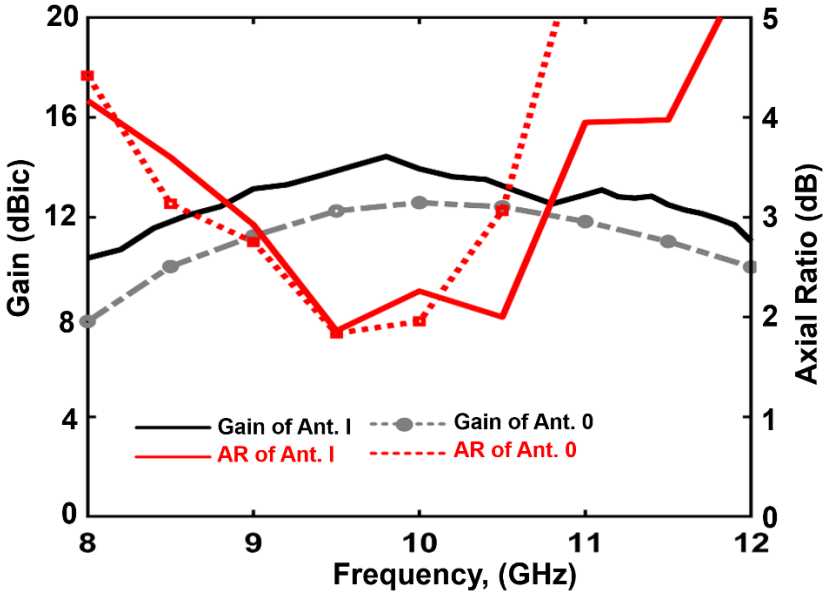

Fig. 7 Simulated antenna gain and the axial ratio of Ant. 0 and Ant. I for excitation of port #1.

Ant. II includes PRS superstrate and the optimized height of the PRS superstrate is $h_r = 12.5$ mm, which is about half wavelength at center frequency. Fig. 13 shows when ports #1 is excited the impedance bandwidth of Ant. I is 3.4 GHz from 8.26 GHz to 11.66 GHz, and when port #2 is excited the impedance bandwidth is 3.66 GHz from 8.12 to 11.78 GHz. In the case of Ant. II, when either port is excited the impedance bandwidth covers the entire X-band. It is evident that the impedance bandwidth and return loss is improved with inclusion of PRS superstrate.

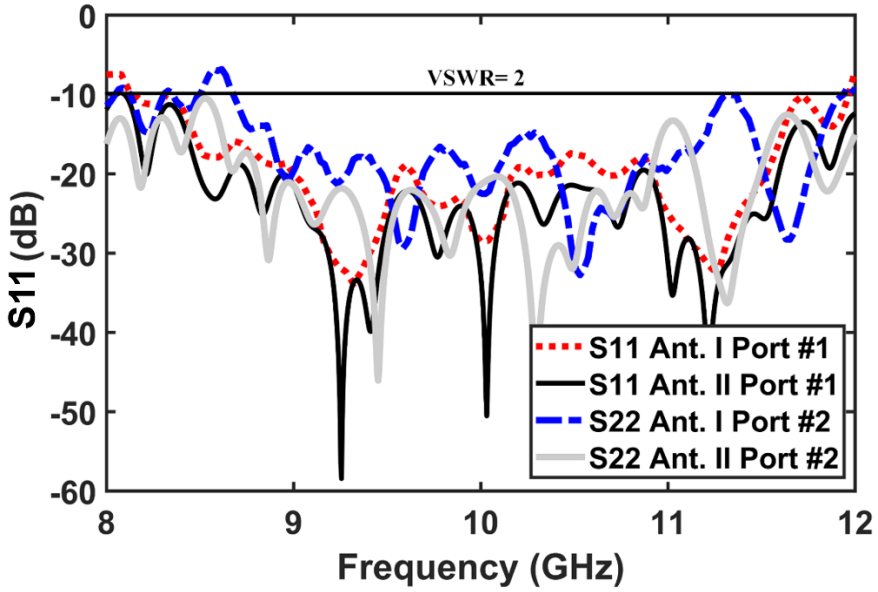

Fig. 8 Simulated return loss of Ant. I and Ant. II when Ports #1 and #2 are excited.

The Fabry-Perot SIW antenna array was constructed based on the above design and its performance measured. The return loss (S_{11} and S_{22}) of Ant. II was measured using a Vector Network Analyzer (Keysight PNA-X N5242A). The simulated and measured scattering parameters are shown in Fig.14. The results show the return loss at ports #1 and #2 cover the whole of the X-band (8-12 GHz). The gain and axial ratio of Ant. II when ports #1 and #2 are excited is shown in Fig.15. The 4×4 Butler Matrix system is constructed using the 1×4 antenna array. The structure looks different because PRS structure is placed above the 4×4 Butler Matrix. The gain is better than 15.9 GHz over the entire X-band and it is approximately flat between 9 GHz and 11 GHz with an average value of 18.6 dBic. The measured axial-ratio bandwidth when port #1 is excited is 3.4 GHz from 8.1-11.5 GHz, and 3.15 GHz from 8.25-11.40 GHz when port #2 is excited. These results prove that using the PRS superstrate leads to a significant increase in circular polarization purity.

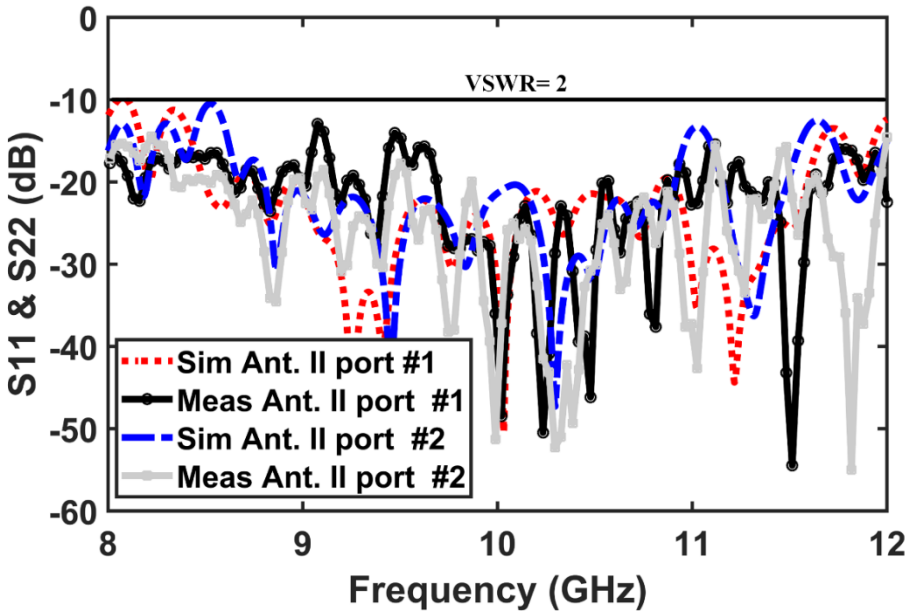

Fig. 14 Simulated and measured return loss for Ant. II when ports #1 and #2 are excited.

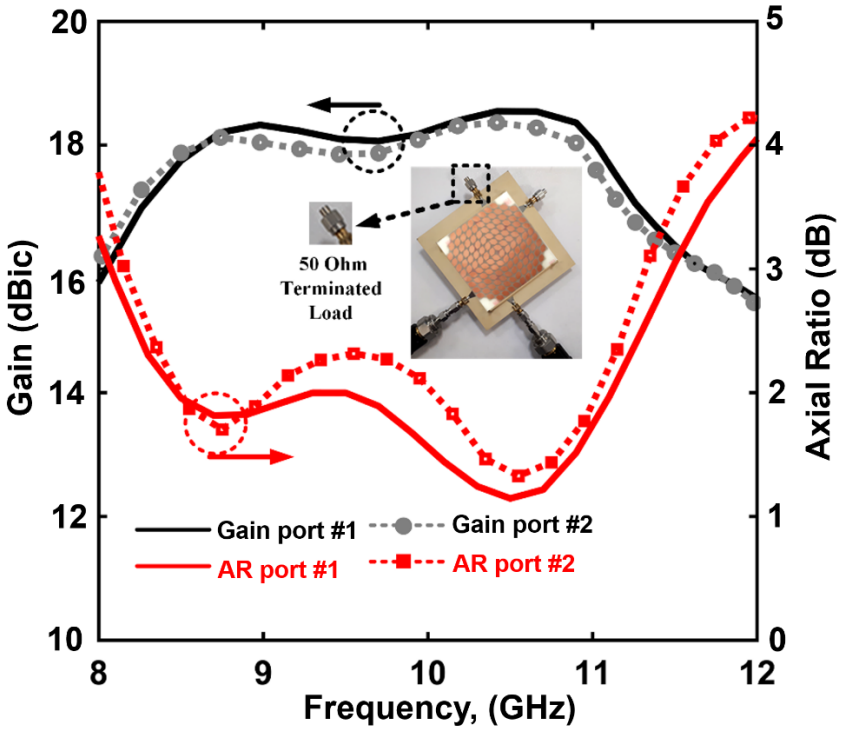

Fig. 9 Measured gain and axial ratio of FPRSAA when ports #1 and #2 are excited.

The radiation patterns of Ant. I and Ant. II at 10 GHz are shown in Fig. 16. It is clear from the figure that the PRS superstrate causes the antenna beamwidth to be more defined and narrower. The radiation pattern of the proposed FPRSAA is capable of scanning between -47 to 47 degrees in the X-band. In Fabry-Perot antenna arrays the antenna beams are typically not orthogonal. This

is the case here, e.g., in Fig.16(a) the phase between ports 1 & 4 is 73 degrees, and between ports 2 & 3 is 63 degrees. The reason can be attributed to factors such as mutual coupling. In practice, the elements in an antenna array are not completely isolated from each other. There is typically some level of mutual coupling between adjacent elements. This coupling can cause interference and lead to correlations between the radiation patterns of different elements, resulting in non-orthogonal beams. The other reason is due to imperfections in design and fabrication. The manufacturing process and practical limitations can introduce imperfections in the antenna array elements and the beamforming network. These imperfections can lead to deviations from the ideal orthogonal radiation patterns. We have clarified this in the revised manuscript.

The proposed antenna array is compared with other reported 2-D scanning antenna systems reported in the literature in Table II. Apart from [33] the proposed antenna array has the widest impedance bandwidth and highest peak gain. However, compared to other works the proposed antenna array has the widest circular polarization range and the widest scanning range.

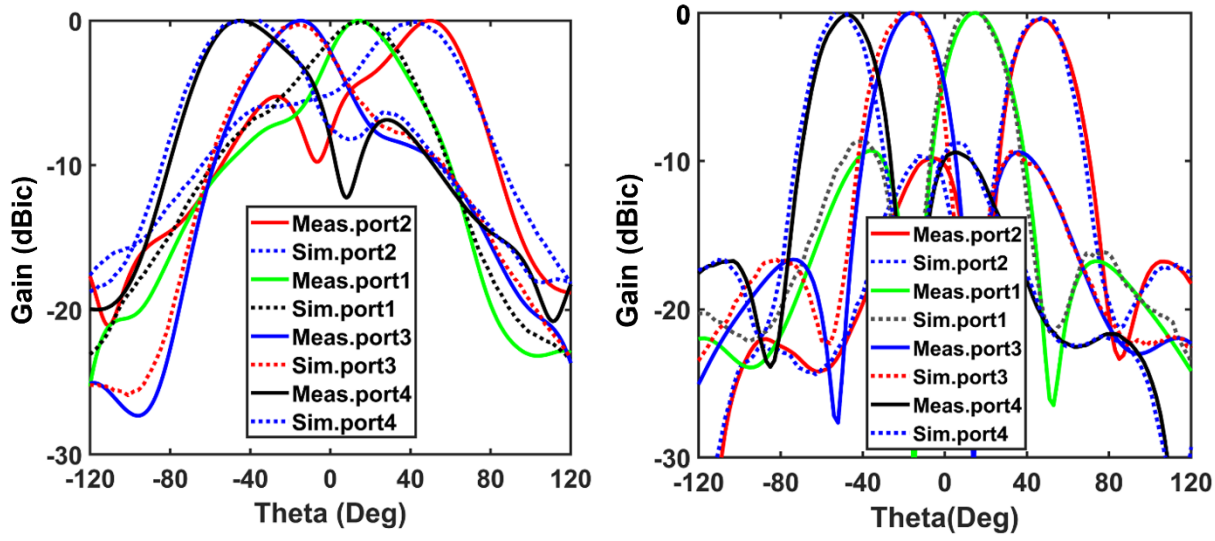

(a) (b)

Fig. 10 Measured and simulated normailized radiation pattern, (a) Ant. I, and (b) Ant. II, when the ports of are excited simultanously.

Table I Comparison between this work and related previous works.

Parameters	[1]	[2]	[31]	[32]	[33]	This work
Feed network type and technology	Butler matrix 3×3 SIW	Butler matrix 4×4 SIW	Butler matrix4×4 microstrip	Butler matrix 4×4 microstrip	Butler matrix 4×4 microstrip	Butler matrix 4×4 SIW
Number of elements	3	4	4	4	4	4
Operating freq. (GHz)	15.25	26.5	35	5.5	35	10
Impedance bandwidth range (GHz)	13-17.5	25.5-27.5	33.8-36.5	4.2-7.5	32.11-37.86	8-12
Fabry-Perot configuration	✓	×	✓	✓	✓	✓
Peak gain (dBic)	14.2	12.9	17.6	14.38	18.9	18.54
Circular polarization range (GHz)	N/A	N/A	×	5-6.6	×	8.5-11
3 dB gain bandwidth range (GHz)	5-6.18z	25- 27	N/A	4.93-6.61	N/A	8-12
Scan range (degrees)	-39 to 38	-38 to 38	-47 to -46	-40 to 40	-46.5-46.5	-47 to 47

5. Conclusion

The design of an innovative beam-switched SIW antenna array is practically verified for X-band applications. The proposed antenna array consists of a modified ring patch antenna, a SIW Butler Network, UC-EBG unit cells separating the radiating elements, and a PRS superstrate. To demonstrate the improvement of the array antenna performance, three different antenna array configurations were designed, namely, Ant. 0, Ant. I and Ant II. The use of a PRS superstrate, UC-EBG structures, and a feeding network, is shown to increase the axial ratio and 3 dB gain bandwidth of the array. The final antenna array (Ant. II) has an impedance bandwidth that covers the entire X-band (8-12 GHz). The circular polarization property is achieved between 8.1 and 11.5 GHz. The gain of the proposed antenna is almost flat across 8.5 GHz to 11 GHz, while 3 dB gain bandwidth covers the entire X-band with peak gain of 18.2 dBic. Four beams firing in different directions were obtained by exciting each feed network ports to provide scanning between -47 and 47 degrees.

6. References

[1] R. K. M. Lou, M. Naser-Moghadasi and R. A. Sadeghzadeh, Broadband Planar Aperture-Coupled Antenna Array for WLAN and ITS Beam-Steering Applications. Radio Science. 2018; 53(2): 200-209

[2] P. Chen et al., A Multibeam Antenna Based on Substrate Integrated Waveguide Technology for MIMO Wireless Communications. IEEE Transactions on Antennas and Propagation. 2009;57(6):200-201813-1821

[3] Fathalizadeh, M, Sedghi, T, Asadpor, L, Zehforoosh, Y, A Compact Size Wide-Angle 3×3 Substrate Integrate Waveguide Butler Matrix for Ku-Band Applications. Int J RF Microwave Computer Aided Eng. 2022; e23120

[4] Y. J. Cheng et al., Substrate Integrated Waveguide (SIW) Rotman Lens and its Ka-Band Multibeam Array Antenna Applications. IEEE Transactions on Antennas and Propagation. 2008;56(8): 2504-2513

[5] Ahn, B., Hwang, IJ., Kim, KS. et al. Wide-Angle Scanning Phased Array Antenna using High Gain Pattern Reconfigurable Antenna Elements. Sci Rep 9. 2019: 18391

[6] S. Karamzadeh, V. Rafii, M. Kartal and B. S. Virdee, Compact and Broadband 4×4 SIW Butler Matrix with Phase and Magnitude Error Reduction, IEEE Microwave and Wireless Components Letters. 2015; 25(12): 772-774

[7] G. Sharifi, Y. Zehforoosh, T. Sedghi, M. Takrimi, A High Gain Pattern Stabilized Array Antenna Fed by Modified Butler Matrix For 5G Applications. AEU - International Journal of Electronics and Communications. 2020;122: 1532-1537

[8] T. Aribi, M. Naser-Moghadasi, and R.A. Sadeghzadeh, Broadband Circularly Polarized Beam-Steering Antenna Array for Wireless Applications. Microw. Opt. Technol. Lett. 2014;56: 2813-2816

[9] D. Tarek, N.J.G. Fonseca, and K. Wu, Design and Implementation of a Planar 4×4 Butler Matrix in SIW Technology for Wide Band High Power Applications. Progress in Electromagnetics Research B. 2011;35: 29-51

[10] Z. Li, T.L. Zh, B. Xu, S. Zheng, Flexible Millimeter-Wave Butler Matrix Based on the Low-Loss Substrate Integrated Suspended Line Patch Hybrid Coupler with Arbitrary Phase Difference and Coupling Coefficient. Int J RF Microw. Comput. Aided Eng. 2021;31:1654-1674.

[11] T. Djerafi, N. J. G. Fonseca and K. Wu, Planar Ku-Band 4×4 Nolen Matrix in SIW Technology. IEEE Transactions on Microwave Theory and Techniques. 2010;58(2): 259-266

[12] H. Ren, H. Zhang, Y. Jin, Y. Gu and B. Arigong, A Novel 2-D 3×3 Nolen Matrix for 2-D Beamforming Applications. IEEE Transactions on Microwave Theory and Techniques. 2019;67(11): 4622-4631

[13] K. Ding and A. A. Kishk, 2-D Butler Matrix and Phase-Shifter Group. IEEE Transactions on Microwave Theory and Techniques. 2018;66(12): 5554-5562

[14] Djerafi, T. and Wu, K. (2012), Multilayered substrate integrated waveguide 4×4 butler matrix. Int. J. RF and Microwave Comp Aid Eng. 2012;22: 336-344

[15] M. Bozzi, Substrate integrated waveguide (SIW) technology: New research trends for low-cost and eco-friendly wireless systems. IEEE MTT-S International Microwave Workshop Series on Millimeter Wave Wireless Technology and Applications, 2012: 1-1

[16] S. Dey, N. S. Kiran and S. Dey, SIW Butler Matrix Driven Beam Scanning Array for Millimeter Wave 5G Communication. 2020 IEEE Asia-Pacific Microwave Conference (APMC). 2020: 709-711
[17] T. Aribi, M. Naser-Moghadasi, R. Sadeghzadeh, Circularly Polarized Beam-Steering Antenna Array with Enhanced Characteristics Using UC-EBG Structure. International Journal of Microwave and Wireless Technologies. 2016;8(6): 955-962
[18] Mohamadzade, B. and Afsahi, M., Mutual Coupling Reduction and Gain Enhancement in Patch Array Antenna Using A Planar Compact Electromagnetic Bandgap Structure. IET Microw. Antennas Propag., 2017;11: 1719-1725
[19] B. Zhu, Y. Feng, Z. N. Chen and T. S. P. See, Fabry-Perót cavity antenna with beam switching. IEEE Asia-Pacific Conference on Antennas and Propagation, 2012: 261-262
[20] A. K. Singh, M. P. Abegaonkar and S. K. Koul, High-Gain and High-Aperture-Efficiency Cavity Resonator Antenna Using Metamaterial Superstrate. IEEE Antennas and Wireless Propagation Letters. 2017;16: 2388-2391
[21] T. Sedgeechongaraluye-Yekan, M. Naser-Moghadasi, and R.A. Sadeghzadeh, Reconfigurable wide band circularly polarized antenna array for WiMAX, C-Band, and ITU-R Applications with Enhanced Sequentially Rotated Feed Network. Int J RF and Microwave Comp Aid Eng. 2015;25: 825-833
[22] S.A. Muhammad, R. Sauleau, L.L. Coq and H. Legay, Self-Generation of Circular Polarization Using Compact Fabry–Perot Cavity Antennas. IEEE Antennas and Wireless Propagation Letters. 2011;10: 907-910
[23] F. Meng, S.K. Sharma, A Wideband Resonant Cavity Antenna with Compact Partially Reflective Surface. IEEE Trans. Antennas Propag. 2019, (68): 1155–1160.
[24] L. Leger, C. Serier, R. Chantalat, M. Thevenot, T. Monedière, B. Jecko, 1D dielectric electromagnetic band gap (EBG) resonator antenna design. Annales des télécommunications 2004, (59): 242–260.
[25] E. Ghahramani, R. A. Sadeghzadeh, B. Boroomandisorkhabi and M. H. Kolagari, Mutual Coupling Reduction in Waveguide-Fed Slot Array Antenna Using Uniplanar Compact EBG (UC-EBG) structure. 2013: 634-636.
[26] Ghosh, C.K., Pratap, M., Kumar, R. et al., Mutual Coupling Reduction of Microstrip MIMO Antenna Using Microstrip Resonator. Wireless Pers Commun. 2020;112: 2047–2056.
[27] Xu-bao Sun, Mao-yong Cao, Mutual Coupling Reduction in an Antenna Array by Using Two Parasitic Microstrips. AEU - International Journal of Electronics and Communications. 2017;74: 1-4.
[28] H. Moghadas, M. Daneshmand, P. Mousavi, Single-Layer Partially Reflective Surface for an Orthogonally Polarized Dual-Band High-Gain Resonant Cavity Antenna. IET Microw. Antennas Propag. 2013;7(8): 656–662.
[29] H. Moghadas, M. Daneshmand, P. Mousavi, Analysis of Radiation of Antennas with a Phase-Gradient Partially Reflective Surface. IET Microw. Antennas Propag. 2015;9(12): 1323–1330.
[30] K.M. Lou, and M. Naser-Moghadasi, Wideband Aperture-Coupled Antenna Array Based on Fabry–Perot Resonator for C-band Applications. IET Microw. Antennas Propag. 2017;11: 859-866.
[31] M. Mbaye, L. Talbi, S. Louati, K. Hettak, and H. Boutayeb, X-Band Multilayer Butler Matrix and SIW Multi-Beam Antenna: Analysis and Design. Progress In Electromagnetics Research M. 2022;107: 79-89.
[32] G. Sharifi, Y. Zehforoosh, T. Sedghi, M. Takrimi, M. Circularly Polarized Beam Steering Array Antenna Fed by Low Magnitude and Phase Error Response of Butler Matrix to Use Pattern Stabilization Applications. Int. J. RF Microw. Comput. Aided Eng. 2022; 32(3):e23022.
[33] S. Karamzadeh, V. Rafiei, M. Kartal, Beam Steering Fabry Perot Array Antenna for mm-Wave Application. Progress in Electromagnetics Research M, 2020, 91: 81-89.
[34] A. Bakhtiari, R. Sadeghzadeh, & M. Naser-Moghaddasi, Millimeter-Wave Beam-Steering High Gain Array Antenna by Utilizing Metamaterial Zeroth-Order Resonance Elements and Fabry-Perot Technique. Int. Journal of Microwave and Wireless Technologies, 2018, 10(3), 376-382.